Proceedings of the Fifteenth International Conference on
Computational Structures Technology
Edited by: P. Iványi, J. Kruis and B.H.V. Topping
Civil-Comp Conferences, Volume 9, Paper 10.8
Civil-Comp Press, Edinburgh, United Kingdom, 2024
ISSN: 2753-3239, doi: 10.4203/ccc.9.10.8

Fractional Calculus in Describing the Viscoelastic Response of PVB foil

M. Šejnoha

Department of Mechanics, Faculty of Civil Engineering
Czech Technical University in Prague, Czechia

Abstract

This paper is concerned with a theoretical description of a polyvinyl butyral (PVB) foil, which is commonly used as an interlayer of laminated-glass composites. This polymer exhibits a significant time and temperature-dependent behaviour and can be effectively described employing the theory of viscoelasticity. The present study concentrated on the ability of both standard and fractional Maxwell chain models to represent the polymer behavior observed experimentally. Both models were calibrated adopting the same set of laboratory data derived with the help of a dynamic shear rheometer for the selected range of frequencies and temperatures. The time temperatures superposition principal was exploited to extend the data beyond the allowable frequency range. The optimal model parameters were then obtained by matching the measured and theoretically predicted response of the polymer in the framework of least squares method. We have seen that the model based on fractional calculus not only requires less number of model parameters but it also provides predictions which are closer to a real behavior of the examined polymer. This promotes its application in smoothing the measured data and consequently allows us to extend the measured domain with a relatively low number of model parameters.

Keywords: viscoelasticity, fractional viscoelasticity, Maxwell chain model, laminated glass, polymer interlayer, PVB foil, rheometer experiment

1 Introduction

The concept of linear small-strain elasticity assumes that the stress σ is proportional to the strain ε, i.e. $\sigma = E\varepsilon$. Similarly, in the case of a pure viscous material, the stress is proportional to the strain rate, i.e. $\sigma = \eta\dot{\varepsilon}$, where constants E and η are material parameters. Because the response of a viscoelastic material is found somewhere in between, it seems natural to generalize this relationship by stating that the stress is directly proportional to the α-derivative of strain, where $\alpha \in \mathbb{R}$. This technique is not common in engineering practice, but for many materials it is more natural and gives better results.

In this contribution, we therefore focus on the applicability of fractional calculus in viscoelasticity with particular application to a polymer interlayer in a laminated glass. Laminated glass is a modern widely used material, where a proper description of the behavior of the interlayer plays a crucial role in a reliable prediction of the behavior of the entire laminate. It has been observed that the approach exploiting fractional calculus allows for a correct description of a gradual creep at long times as well as it provides a correct estimate of dissipated energy in faster processes. A classical rheological formulation is not so flexible in simultaneously describing fast and slow events. Thus to describe an entire life cycle of a material requires using a large number of rheological cells. The fractional model is much more flexible and natural in this regard. This will be presented in light of a calibration step of a standard and fractional Maxwell chain model to represent experimental data acquired from a rheometer test.

The theoretical background of fractional calculus is briefly described in Section 2 whereas a short note on the performed laboratory measurements is provided in Section 3. The measured data, summarized in Section 4, are subsequently adopted in the calibration step addressed in Sections 5 and 6. The essential outcomes are finally discussed in Section 7.

2 Fractional viscoelasticity

In fractional viscoelasticity the viscous behavior is represented by a springpot element, see ahead Fig. 6(b), which relates the stress to the strain rate in the form

$$\sigma(t) = \xi D^{\alpha}\varepsilon(t), \tag{1}$$

where α and ξ are parameters of the model and D^{α} is a noninteger derivative. Two limit cases can be defined to arrive either at a spring element with ξ representing the Young modulus E when setting $\alpha = 0$ or at a dashpot element with $\alpha = 1$ to associate ξ with the viscosity η. An auxiliary ratio $\tau = \eta/E$ is called the characteristic time. With this parameter it becomes profitable to write the stress-strain relation (1) as

$$\sigma(t) = E\tau^{\alpha}D^{\alpha}\varepsilon(t), \tag{2}$$

which directly leads to the above mentioned limit cases, see [4] for more details.

An underlying principle of fractional integration is a generalization of the Cauchy formula for repeated integration

$$J^n f(t) = \frac{1}{(n-1)!} \int_0^t (t-t')^{n-1} f(t') \, \mathrm{d}t', \quad n \in \mathbb{N},$$

where J^n denotes the integration of the order of n. The gamma function Γ allows us to move to a space of real numbers $\mathbb{R}$ to get

$$J^\alpha f(t) = \frac{1}{\Gamma(\alpha)} \int_0^t (t-t')^{\alpha-1} f(t') \, \mathrm{d}t', \quad \alpha \in \mathbb{R}.$$

The definition of α-th derivative is typically based on the definition of fractional integral J^α. The two commonly used formulations, which provide identical results, are:

Riemann-Liouville fractional derivative is defined as

$$D^\alpha_{RL} f(t) = D^{\lceil \alpha \rceil} J^{\lceil \alpha \rceil - \alpha} f(t), \tag{3}$$

where D^n denotes n-th differentiation and $\lceil \bullet \rceil$ is the ceiling function. For example, if we wish to differentiate a function $f(t)$ 0.8 times, we first integrate this function 0.2 times and after that we take the first derivative of the result, which is mathematically written as

$$D^{0.8} f(t) = D^1 J^{0.2} f(t). \tag{4}$$

Caputo fractional derivative is defined in the same way, only the order of differentiation and integration is reversed, i.e.,

$$D^\alpha_C f(t) = J^{\lceil \alpha \rceil - \alpha} D^{\lceil \alpha \rceil} f(t), \tag{5}$$

which, for the above example, gives

$$D^{0.8} f(t) = J^{0.2} D^1 f(t). \tag{6}$$

3 Experimental analysis of PVB foil

In the present study we limit our attention to a PVB (polyvinyl butyral) polymer interlayer as the most typical interlayer used in laminated glasses. Apart from ensuring interaction of individual glass plates it also dissipates a portion of energy when subjected, e.g., to impact or blast loading. For the laminated glass element in bending the interlayer is loaded mostly in shear. Obtaining shear properties of a material experimentally can be accomplished for example via a dynamic shear rheometer. By

Figure 1: Dynamic shear rheometer Malvern KINEXUS

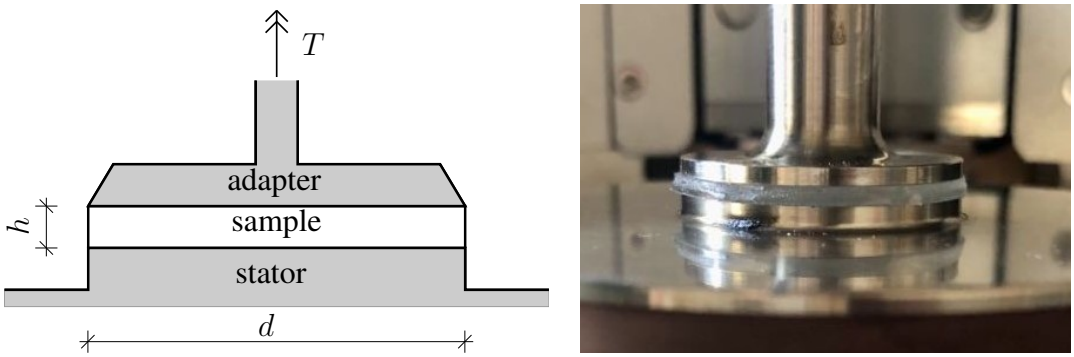

(a) (b)

Figure 2: Parallel-plate rheometer with attached sample – (a) scheme, (b) photograph

loading the material in a simple torsion this device allows for determining both elastic and viscous properties.

The Malvern KINEXUS DSR+ rheometer adopted in our study is displayed Fig. 1. It utilizes a parallel-plate geometry schematically plotted in Fig. 2 (a). Figure 2 (b) shows the photograph of the same configuration. The sample is attached between the two parallel plates. The upper plate, termed adapter, can move along and rotate around the vertical axis perpendicular to the plate. The bottom plate, called stator, is fixed. The torsional load is introduced to a sample via rotation of the adapter. The loading process can be controlled either by the shear stress or by the shear strain and the rheometer can perform static loading (e.g. the creep test) or the dynamic loading. An application of a dynamic rheometer apparatus to laminated glass samples is presented in [1]. In the present study, however, the load is introduced directly to the polymer foil as also seen in Fig. 2 (b).

The sample is loaded by a harmonic (sinusoidal) strain while the stress response is monitored by the rheometer. The software then extracts the values of amplitudes of the strain γ_0 and the stress τ_0 and the phase shift δ between the load and the response. These values are converted into the required outputs – the storage modulus G', the loss modulus G'', and the complex modulus G^*. These moduli are given by

$$\begin{aligned} G'(\omega) &= \frac{\tau_0}{\gamma_0} \cos\delta, \\ G''(\omega) &= \frac{\tau_0}{\gamma_0} \sin\delta, \\ G^*(\omega) &= G'(\omega) + iG''(\omega). \end{aligned} \tag{7}$$

The rheometer outputs are based on the known diameter of the rheometer plates d and the gap between the plates, which corresponds to the thickness of the sample h. The rheometer software assumes that the sample is perfectly filling the gap between the plates as is shown in Fig. 2 (a), i.e., the same diameter $d = 25$ mm of the sample and of the plates is considered and the sample is homogeneous over its height. Material samples of two different thicknesses, 0.76 mm and 1.52 mm, were examined. The samples were attached to the rheometer plates employing high temperature and compressive force introduced by the adapter.

The dynamic moduli were determined via frequency sweep test with the prescribed amplitude of shear strain equal to 0.1 %. The measurements were performed for frequencies in the range of 0.01-100 Hz (approximately 0.0628-628) rad/s and for multiple different temperatures in the range of 0-100 °C. Further details can be found [2].

4 Results from rheometer

This section presents the storage and loss moduli obtained from the rheometer experiment. The graphs in Fig. 3 show the results obtained for one measured sample, specifically the 0.76 mm sample laminated at 140 °C. It is evident that for frequencies over 200 rad/s (approximately 32 Hz) and under 0.2 rad/s (0.032 Hz) the results are very volatile and unreliable. This is probably caused by meeting the limits of the measuring device. This phenomenon was significant for every measurement. Therefore, this range of frequencies was excluded from further analyses. These deviations are even more pronounced for the loss modulus, see Fig. 3, especially for the results obtained for temperatures under 20 °C. Figure 4 shows the average values of the obtained moduli for both thicknesses of the tested material. The results clearly show the frequency and temperature dependence of the storage and loss moduli.

When the results for the storage modulus are analysed, it is obvious that the values of the modulus are higher for lower temperatures and vice versa. Therefore, the response of the material is stiffer for lower temperatures and more compliant for higher

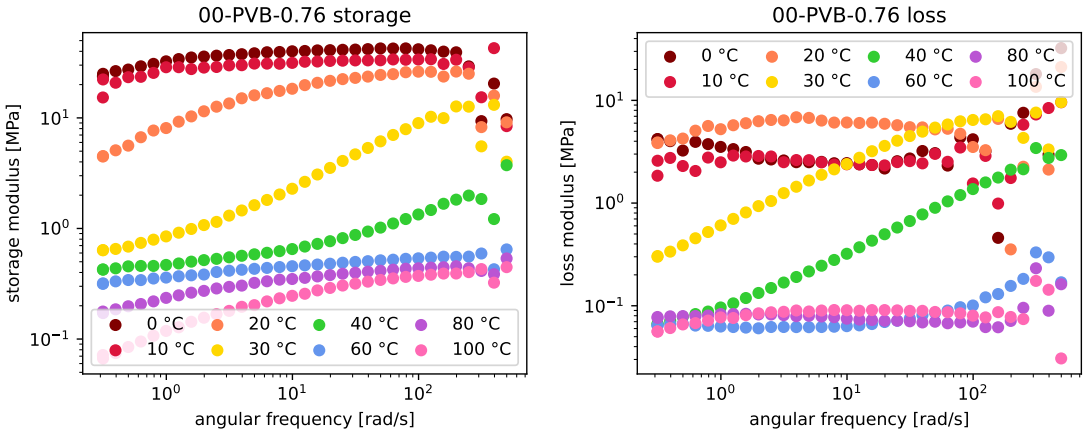

(a) (b)

Figure 3: Experimental results on 0.76 mm PVB foil laminated at 140 °C for (a) storage modulus, (b) loss modulus

temperatures. This phenomena is mostly noticeable for temperatures between 20-40 °C. For this temperature range we also see the most significant dependence on frequency – for a rapid loading (high frequencies) the material is stiffer then for a slow loading (low frequencies). For temperatures under 10 °C and around 60 °C the frequency dependence is less significant which refers to a solid-like behaviour of the material for these temperatures.

As for the loss modulus, we see that the frequency dependence is mostly noticeable for temperatures between 20-40 °C as well. For other measured temperatures the results are almost constant over the selected frequency range. Temperature dependence of the loss modulus is also important. However, for temperatures in the range of 60-100 °C there is no significant difference and the values of the loss modulus are similar. With decreasing temperature the loss modulus initially increases. Nevertheless, in the range of temperatures between 0 and 10 °C we observe an opposite trend. The values of the modulus in this temperature range are lower than for 20 °C and for some measurements even for 30 °C, especially for higher frequencies. Because of this unclear behaviour the following analysis is focused on the storage modulus only, while the loss modulus measurements will require further research.

5 Time-temperature superposition principle

The time-temperature superposition principle assumes that the viscoelastic behaviour examined for one temperature can be related to the behaviour for another temperature when its timescale is changed [3]. In other words, from the set of measurements for various temperatures we can establish one temperature as a reference T_{R} and all of the measurements results can be related to T_{R} by changing their time (or, in our case, frequency) domain.

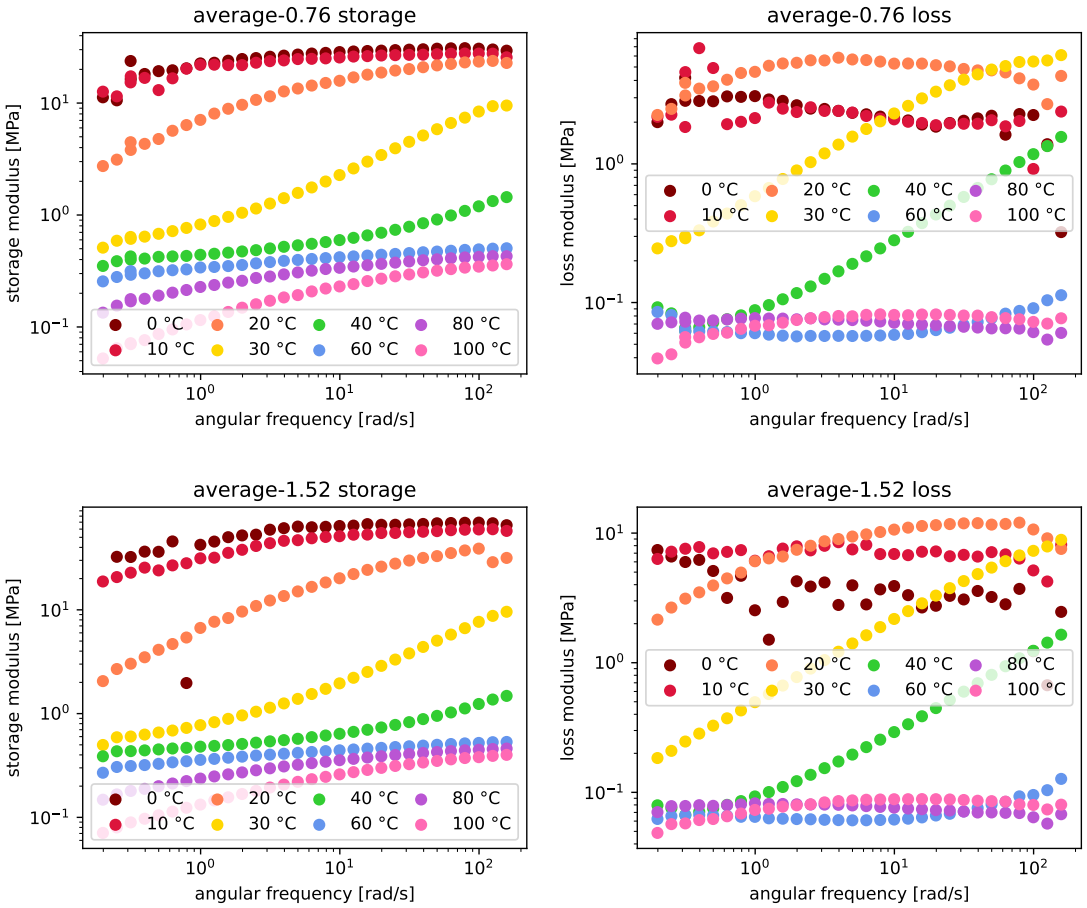

(a) (b)

Figure 4: Average results for 0.76 mm and 1.52 mm PVB foil for (a) storage modulus, (b) loss modulus

For example, we have the storage modulus G' depending on frequency ω and temperature T. The frequency and temperature can be tied by the shift factor α_{R} related to the reference temperature T_{R}. Since the reference temperature is set, the shifted function then depends only on frequency,

$$G'(\omega, T) \quad \rightarrow \quad G'(\alpha_{\mathrm{R}}\omega, T_{\mathrm{R}}). \tag{8}$$

This result is then related to the reference temperature $T \equiv T_{\mathrm{R}}$ and provides an extension of the measured range in the frequency domain. This extended curve for temperature T_{R} is called a mastercurve.

The shift is obtained by multiplying the original frequency range ω by the shift factor α_{R} which, in the logarithmic scale, results in a horizontal shift of the curve only. The shift factor depends on the original temperature T and it can be obtained

from the Williams-Landel-Ferry (WLF) equation in the form [3]

$$\log \alpha_{\mathrm{R}}(T) = \frac{-C_1(T - T_{\mathrm{R}})}{C_2 + T - T_{\mathrm{R}}}, \tag{9}$$

where $\log$ denotes a decadic logarithm and $C_1,\ C_2$ are parameters that need to be found for the specific set of results so the shifting provides the smoothest possible mastercurve. The parameters are optimized based on the least squares method. The optimization compares the data points corresponding to the different temperatures and their deviations over the current overlapping region. If we have a set of measurements for more than two temperatures the whole set is then described by the same WLF equation and to find the optimal parameters $C_1,\ C_2$ all curves are exploited at once. The optimization was performed using the fminbnd function in MATLAB.

An illustrative example of the mastercurve fitting is shown in Fig. 5 for the average results measured on 1.52 mm sample. The grey dashed lines mark the measured frequency domain where we see the originally measured data for various temperatures. The data marked by $\times$ are shifted relative to the reference temperature $T_{\mathrm{R}} = 20$ °C with the optimized parameters of WLF equation $C_1 = 14.7231,\ C_2 = 120.7819$ °C. We see that the shift provides a significantly extended frequency domain.

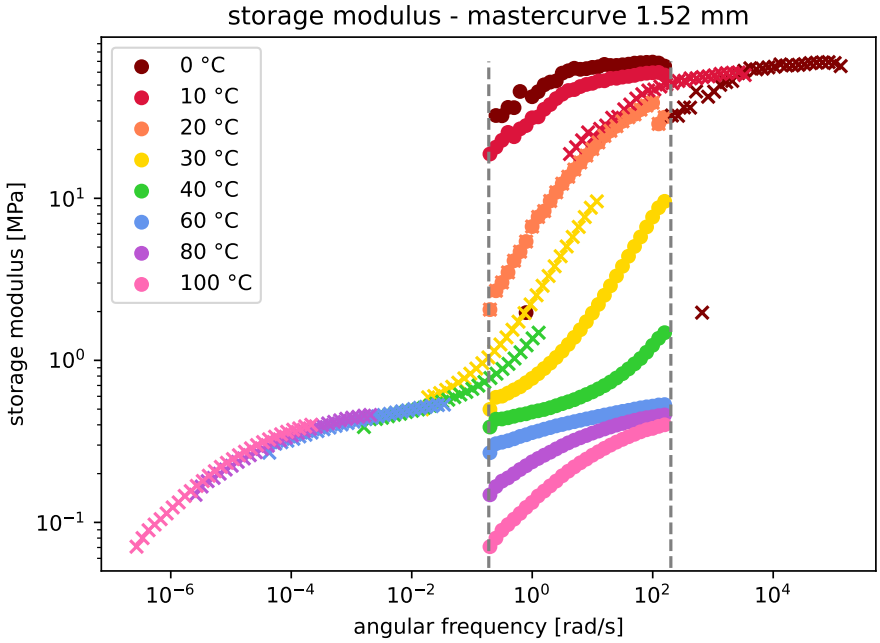

Figure 5: Example of mastercurve fitting

6 Approximation of the measured data

To appreciate a potential advantage of fractional calculus we compare approximation of the measured data provided by the standard Maxwell chain model in Fig. 6(a) and by the fractional Maxwell chain model in Fig. 6(b).

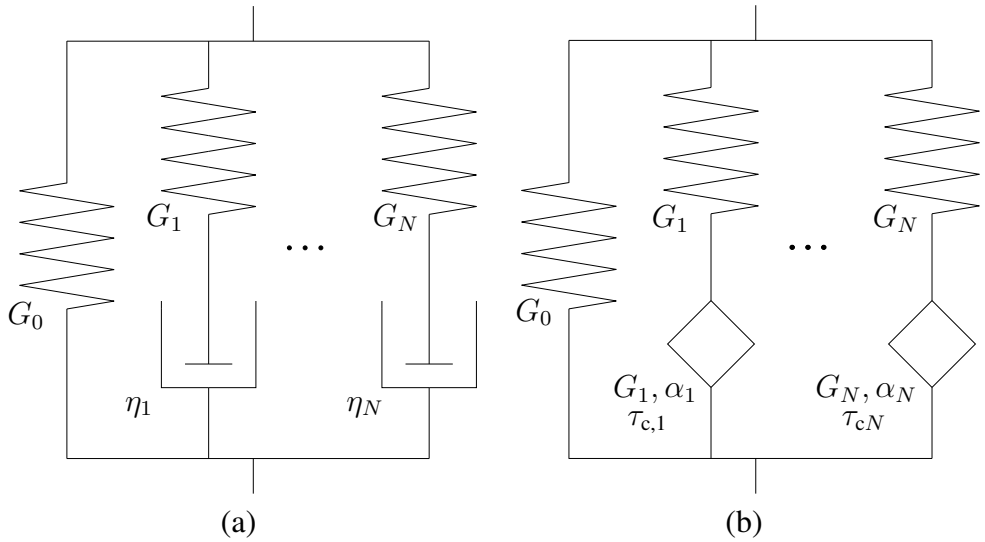

Figure 6: (a) Standard Maxwell chain model, (b) Fractional Maxwell chain model

Mathematically, the storage modulus of the standard model is provide by

$$G'(\omega) = G_0 + \sum_{i=1}^{N} \frac{G_i \omega^2 \tau_{ci}^2}{\omega^2 \tau_{ci}^2 + 1}, \tag{10}$$

whereas the storage modulus associated with the fractional model reads

$$G'(\omega) = G_0 + \sum_{i=1}^{N} G_i \frac{(\tau_{ci}\omega)^{2\alpha_i} + (\tau_{ci}\omega)^{\alpha_i} \cos\left(\alpha_i \frac{\pi}{2}\right)}{(\tau_{ci}\omega)^{2\alpha_i} + 2(\tau_{ci}\omega)^{\alpha_i} \cos\left(\alpha_i \frac{\pi}{2}\right) + 1}, \tag{11}$$

where N stands for the number of cells.

When constructing the standard model we considered one Maxwell cell per each decade in the range of frequencies we wanted to describe. This suggested a 12-cells model with the characteristic times τ_{ci} set as

$$\tau_{ci} = 10^j, \quad j = \{-5,\ -4,\ \ldots,\ 6\}, \quad N = 12.$$

The remaining parameters, i.e., the moduli G_i of individual cells and the eleastic modulus G_0, were then optimized exploiting again the experimentally obtained mastercurve in Fig. 5. The resulting parameters are summarized in Tab. 1. Ability of this model to approximate the experimental data is shown in Fig. 7.

For the fractional model the characteristic times were also selected with respect to the examined range of frequencies. The chosen values comply with the shape of the experimentally observed mastercurve. In particular, they correspond to the frequencies where the slope of the curve changes. The characteristic times τ_{ci} were thus set as

$$\tau_{ci} = 10^j, \quad j = \{-1.5,\ 1,\ 5\}, \quad N = 3.$$

Parameter	Value	Parameter	Value
G_0	0.04625 MPa	G_7	0.8527 MPa
G_1	0.0263 MPa	G_8	4.1315 MPa
G_2	0.09625 MPa	G_9	20.6808 MPa
G_3	0.1266 MPa	G_{10}	9.743 MPa
G_4	0.09871 MPa	G_{11}	15.327 MPa
G_5	0.06262 MPa	G_{12}	18.5988 MPa
G_6	3.534e-11 MPa		

Table 1: Parameters of standard Maxwell chain – 1.52 mm sample, fitting to experimental data

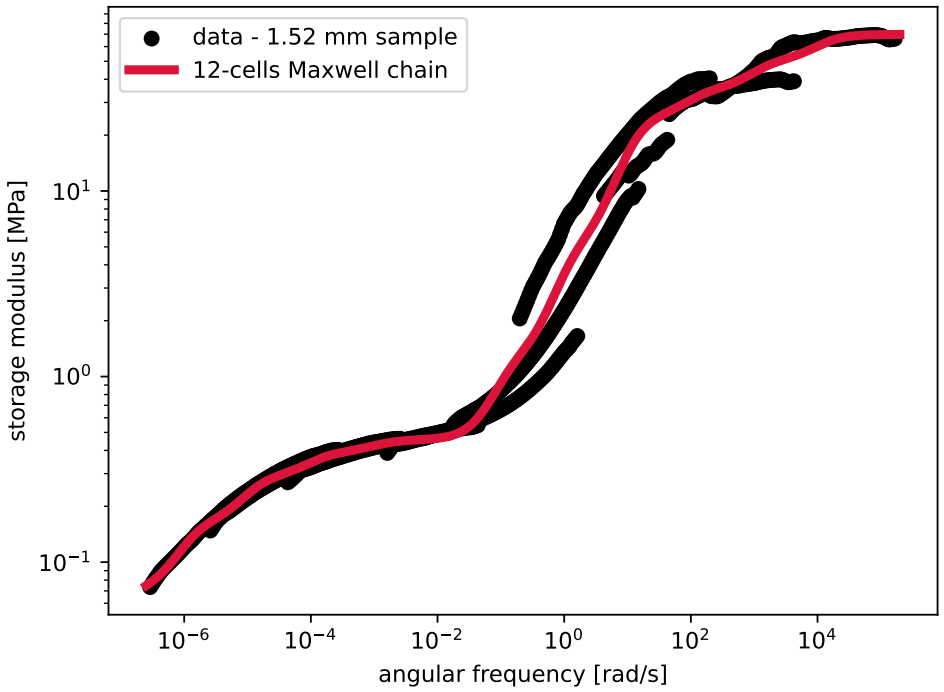

Figure 7: Approximation of the data for 1.52 mm sample by 12-cells standard Maxwell chain with model parameters according to Tab. 1

Parameter	Value	Parameter	Value
G_0	0.0416 MPa	α_1	0.6713
G_1	50.1031 MPa	α_2	0.2161
G_2	0.1563 MPa	α_3	0.5368
G_3	0.3441 MPa		

Table 2: Parameters of fractional Maxwell chain – 1.52 mm sample, fitting to experimental data

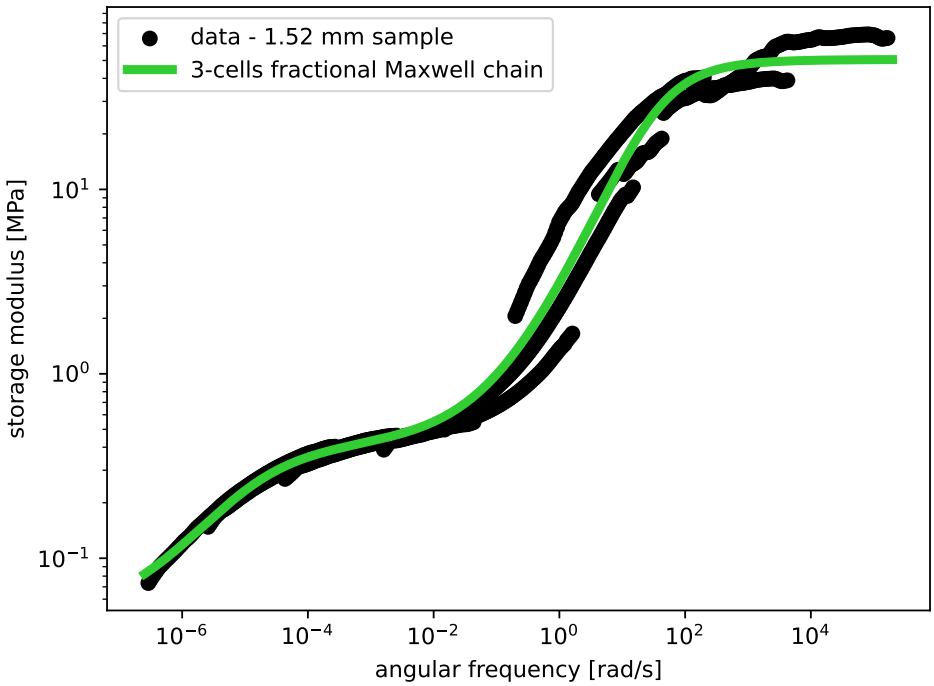

Figure 8: Mastercurve for 1.52 mm sample smoothed using 3-cells fractional Maxwell chain, model parameters according to Tab. 2

The optimized model parameters of the fractional Maxwell chain are summarized in Tab. 2. The approximation of the data set is then plotted in Fig. 8.

Comparing the resulting approximations given by the standard and fractional Maxwell chains clearly shows that the fractional model provides smoother results than the standard model. The number of optimized parameters also differs. While the standard Maxwell chain required 13 parameters to get an acceptable fit, the fractional model yielded suitable approximations for only 7 fitted parameters. We may thus conclude that the fractional model is able to give more accurate approximation in comparison to the standard model with even less parameters to be calibrated. The fractional model can also be efficiently used to smooth and store the experimentally obtained data.

7 Conclusions

Application of fractional viscoelastic models for the description of a polymer interlayer in a laminated glass was examined. While an efficient numerical implementation of such a model is still a subject of an ongoing research, its ability to better capture a physical reality in comparison to standard models is doubtless. Given a relatively low number of tuned model parameters to provide a sufficiently accurate prediction of the material response, it appears advantageous to adopt this model in smoothing and storing the measured data, e.g., in terms of a theoretically provided mastercurve. Thus if needed the model parameters of the standard Maxwell chain model can be then

calibrated to the smoothed mastercurve provided by the fractional Maxwell model.

Acknowledgements

The support provided by the Czech Science Foundation, the grant No. 22-15553S, is gratefully acknowledged.

References

[1] L. Andreozzi, S.B. Bati, M. Fagone, G. Ranocchai, F. Zulli. Dynamic torsion tests to characterize the thermo-viscoelastic properties of polymeric interlayers for laminated glass. Construction and Building Materials 65 (2014): 1-13, DOI: 10.1016/j.conbuildmat.2014.04.003

[2] B. Hálková, Experimental and numerical modelling of PVB foil. MS thesis. Czech Technical University in Prague, Faculty of Civil Engineering. 2024.

[3] I. M. Ward, and J. Sweeney. Mechanical properties of solid polymers. John Wiley & Sons, 2012.

[4] R.C. Koeller. Applications of fractional calculus to the theory of viscoelasticity. Journal of applied Mechanics 51. 1984.

[5] M. Di Paola, L. Galuppi, G.R. Carfagni. Fractional viscoelastic characterization of laminated glass beams under time-varying loading. International Journal of Mechanical Sciences 196. 2021.